J IRAN CHEM SOC (2017) 14:209–219
DOI 10.1007/s13738-016-0971-2

ORIGINAL PAPER

Core–shell thermal-responsive and magnetic molecularly imprinted polymers based on mag-yeast for selective adsorption and controlled release of tetracycline

Wei Ma[1,2] · Songtian Li[1] · Long Chen[2] · Jun Sun[2] · Yongsheng Yan[2]

Received: 17 February 2016 / Accepted: 29 August 2016 / Published online: 1 September 2016

Abstract A novel thermal-responsive and magnetic molecularly imprinted polymers (TMMIPs) were prepared based on mag-yeast via a mild and effective method; the obtained TMMIPs were used for selective adsorption and release of tetracycline from aqueous solution. Imprinted polymerization directly occured on the surface of microspheres, and core–shell imprinted polymers were developed via in situ precipitation polymerization. The properties of obtained TMMIPs were characterized by scanning electron and transmission electron microscopy, X-ray diffraction, Fourier transform infrared spectra, thermo-gravimetric analysis and so on. The adsorption equilibrium data were well described by Langmuir isotherm model. Kinetic experiments showed the adsorption process reached the equilibrium within 60 min, and the pseudo-second-order kinetic model was used to fit the adsorption data well. TMMIPs exhibited magnetic sensitivity, magnetic stability and thermal stability. Reversible recognition and release of template molecule were realized by changing environmental temperatures. Several other antibiotics were selected as model analytes to evaluate the selective recognition performance of TMMIPs. The TMMIPs have good temperature response, selectivity and reusability, making them possible in applying for antibiotics adsorption and controlled release.

Keywords Tetracycline · Thermal-responsive · Magnetic · Molecularly imprinted polymers · Selective adsorption and release

Introduction

Because of good activity and cost effectiveness of tetracycline antibiotics (TC), TC is a commonly used antibiotic to cure several infectious diseases for prevention and treatment of farm animals and promote the growth of livestock as an additive to animal feeds [1–3]. However, TC is very difficult to be completely metabolized and poorly absorbed by the digestive system; their residues in the environment can induce the growth of antibiotic-resistant pathogens and cause harm to human [4, 5]. TC residue is a serious problem that should be concerned because it is not only a threat to human health but also a obstacle to the international trade of the animal products. Thus, it is of great necessity to develop a mild and effective method for the removal of TC residue in the environment.

Nowadays, the ways for removing TC residue include membrane separation, photo-catalysis, electrochemical process, biodegradation and adsorption. However, these methods have their own drawbacks in application. Membrane separation method is influenced by organic material and the dissolved salts in the environment; in addition, the membrane is easy to be blocked causing a higher cost [6, 7]. For photo-catalysis process, the light source with high energy and the higher effective catalysts are required [8, 9], and large-scale application is still restricted [10]. The

Electronic supplementary material The online version of this article (doi:10.1007/s13738-016-0971-2) contains supplementary material, which is available to authorized users.

✉ Yongsheng Yan
253258398@qq.com

[1] School of Chemistry and Chemical Engineering, Pingdingshan University, Pingdingshan 467099, People's Republic of China

[2] Department of Chemical Engineering, School of Chemistry and Chemical Engineering, Jiangsu University, Zhenjiang 212013, People's Republic of China

higher energetic consumption limits the application of the electrochemical process [11]. The environmental factors, such as pH, temperature, oxygen and water, greatly influence the growth and degradation ability of microorganism in biodegradation process [12]. Owing to lower cost, higher effective and environment-friendly adsorption is considered as a practical approach for the removal of TC residue from wastewater in situ [13].

Compared to common adsorbents as active carbon [14] or silica gel [15], selective adsorption using molecularly imprinted polymers (MIPs) appears to be a promising approach for the removal of trace pollutants in the environment [16–18]. The synthesis of a polymer in the presence of a template molecule and the subsequent removal of the template furnish a robust material with "memory" sites, with the ability to selectively rebind the original template from a mixture. MIPs are synthesized with tailor-made binding sites for a template, with which they strongly interact [19], and they have been utilized to selectively remove templates from more complex environmental matrices.

Smart imprinting process is at the head of the MIP technology, showing stimulus-responsive recognition ability from the environment, such as temperature [20, 21], light [22] and pH [23]. In particular, the use of magnetic-sensing and thermo-responsive MIPs as drug delivery systems, sensors and solute separation devices have been studied by many researchers [24]. In many instances, the poly (*N*-isopropylacrylamide) (PNIPAM)-based MIPs showed thermosensitive molecular recognition rooting in the thermal phase transition of PNIPAM [25, 26]. The hydrophilicity of PNIPAM increases with decreasing temperature, which makes PNIPAM swell in water and accessible of analytes to the MIPs at lower temperature. Moreover, another typical example of the stimuli-responsive material is magnetic-sensing; the resulting magnetic molecularly imprinted polymers (MMIPs) could combine the advantages of molecular recognition and fast magnetic separation.

Although smart MIPs own many significant advantages, it still exists many problems such as lower binding capacity, slower mass transfer and difficult template removal. Surface imprinting technology can overcome above drawbacks. The binding sites of MIPs are situated in the surface layer, which can recognize template molecules rapidly and remove them from the binding sites easily. A number of materials are used as a molecularly imprinted technique carrier including membranes, silica particles, graphene, and organic and inorganic materials [27–29].

Compared with the above imprinting supports, the yeast has the advantages of low cost, easily available source [30] and abundant active biomolecule on the cell wall [31] without further modification process. Considering the above advantages, yeast may be chosen as a promising support substrate in the molecularly imprinting process.

In this work, the magnetic composites were prepared by coating the chitosan (CTS) layer containing Fe_3O_4 nanoparticles onto the surface of the yeast. The thermal-responsive and magnetic molecularly imprinted polymers (TMMIPs) based on mag-yeast were prepared by in situ precipitation polymerization. The TMMIPs were prepared by using TC as template molecule, methacrylic acid (MAA) as functional monomer, *N*-isopropylacrylamide (NIPAM) as the thermal-responsive monomer, ethylene glycol dimethacrylate (EGDMA) as cross-linking monomer and AIBN as initiator. The preparation of TMMIPs via precipitation polymerization is schematically illustrated in Fig. 1. The characterization, adsorption capacity and selectivity of TMMIPs were described and discussed in detail.

Experiments

Materials

Yeast powder was purchased from Angel Yeast Co. (Yichang, China). Iron(III) chloride hexahydrate($FeCl_3{\cdot}6H_2O$), iron(II) chloride tetrahydrate($FeCl_2{\cdot}4H_2O$), glutaraldehyde(GA), petroleum ether, isopropanol, ethanol, acetonitrile and chitosan (80.0–95.0 % acetylation degree), liquid paraffin and span-80 were obtained from Sinopharm Chemical Reagent Co., Ltd. (Shanghai, China). Ethylene glycol dimethacrylate (EGDMA, 98 %), 2,2′-Azobis(2-methyl-propionitrile) (AIBN, 99 %), *N*-isopropylacrylamide (NIPAm), methacrylic acid (MAA, 98 %), tetracycline (TC, 98 %), chloramphenicol (CAP, 98 %), ciprofloxacin (CIP, 98 %) and oxytetracycline (OTC, 99 %) were obtained from Aladdin Reagent Co., Ltd. (Shanghai, China). All of the reagents

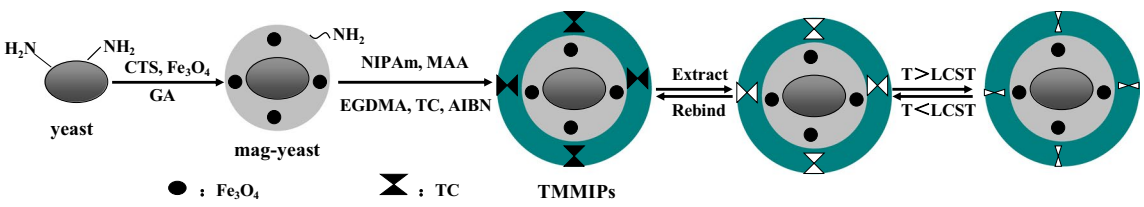

Fig. 1 Synthesis approach of TMMIPs by precipitation polymerization

were of analytical grade. Double-distilled ultrapure water was purified with a Purelab ultra (Organo, Tokyo, Japan).

Preparation of Fe_3O_4 nanoparticles [32]

Fe_3O_4 nanoparticles are prepared by coprecipitating Fe^{2+} and Fe^{3+} ions. Ferric and ferrous chlorides (molar ratio 2:1) were dissolved in the water at 40 °C under N_2; $NH_3{\cdot}H_2O$ solution was added dropwise to prepare iron oxides. The pH of the final mixtures was controlled in the range of 10–11, The whole reaction process was under mechanical agitation. The mixtures were aged at 70 °C for 1.5 h and then washed several times with distilled water until the supernatant pH was neutral. The obtained Fe_3O_4 nanoparticles were dried in a vacuum oven at 60 °C for 12 h.

Preparation of mag-yeast composites

The magnetic composites based on the surface of yeast were prepared as follows [33]. Firstly, 1.0 g of yeast was dissolved in 10 mL of 0.9 % NaCl aqueous solution under a vigorous stirring for 30 min at 25 °C. Then, 2 % (w/v) of CTS solutions were prepared by dissolving 0.8 g of CTS into 40 mL of 0.1 mol L^{-1} acetic acid aqueous solution under ultrasonic stirring for 1.5 h at room temperature. Secondly, 0.2 g of Fe_3O_4 and the yeast solution were added into the CTS colloidal mixture. After stirred for 1.5 h, 150 mL of paraffin oil and 7.5 mL of Span-80 were added into the prepared mixture. After 30 min of emulsification, 6.0 mL of 25 % (v/v) glutaraldehyde as a crosslinking agent was added dropwise into the mixture. Then, the cross-linking reaction was continued for 1.5 h at 40 °C under a nitrogen atmosphere. Next step, the pH of the mixed system was adjusted to 9.0–10 by using 1.0 mol L^{-1} $NH_3{\cdot}H_2O$ and kept in a water bath for a further 1.0 h at 70 °C. Finally, the resulting brown precipitates (mag-yeast) were collected by a Nd–Fe–B permanent magnet. After washing several times by n-hexane, methanol and double distilled water, the mag-yeast was dried at 60 °C under atmospheric condition.

Preparation of TMMIPs by precipitation polymerization

The TC-imprinted polymer nanoshell coated on the surface of mag-yeast was prepared by in situ precipitation polymerization, where MAA, NIPAM and EGDMA were employed as functional monomer, thermosensitive monomer and cross-linking agent, respectively. Briefly, MAA (0.3 mmol), NIPAM (2.25 mmol), EGDMA (1.2 mmol) and TC (0.075 mmol) were dissolved in acetonitrile (50 mL) to self-assemble in the dark at room temperature. Mag-yeast (150 mg) was dispersed into the above solution by ultrasonication, and then, AIBN (10 mg) as the initiator was added. This mixture was purged with nitrogen for 30 min in the ice bath. To ensure homogeneous dispersion of mag-yeast, the reaction was carried out in a water bath oscillator with a rate of 200 rpm. The prepolymerization was first undertaken at 50 °C for 6 h, and the cross-linking polymerization was completed at 60 °C for 24 h. The resulting MIPs were separated from the mixed solution with the help of an external magnet and were then washed with acetonitrile and ethanol several times, with the mole ratio of MAA to EGDMA keeping at a constant value of 1/4. The template TC of the polymers was extracted with a mixture of methanol and acetic acid (9:1, v/v) until no release of TC was detected by UV–Vis spectrum. The corresponding non-imprinted polymers (NIPs) were also synthesized by the identical procedure without the addition of TC template.

Characterization

Fourier transform infrared (FT-IR) spectra were recorded on a Nicolet Nexus 470 FT-IR (America thermo-electricity Company, America) with 2 cm^{-1} resolution in the range 400–4000 cm^{-1}, using KBr pellets. UV–Vis absorption spectra were obtained using a Specord 2450 spectrometer (Shimazu, Japan). X-ray diffraction (XRD) technique was used to characterize the crystal structure of as-prepared microspheres. In this work, XRD patterns were obtained with a D/max-RA X-ray diffractometer (Rigaku, Japan) equipped with Ni-filtrated Cu Ka radiation (45 kV, 200 mA). The 2θ scanning angle range was 10°–80° with a step of 0.02°/0.2 s. The SEM images were examined with S-4800 scanning electron microscopy (HITACHI, Japan). TEM micrographs were taken with a JEOL-JEM-2010 (JEOL, Japan) operated at 200 kV. The thermogravimetric analysis (TGA) of the samples (powdered form, weighing about 5 mg) were performed using a SDT Q600 TG/DTA instrument (TA, American) under a nitrogen atmosphere up to 800 °C with a heating rate of 10 °C min^{-1}. The measurements of magnetic particles were carried out using a vibrating sample magnetometer (VSM, HH-15, China) under a magnetic field up to 10 kOe.

Batch adsorption experiments

The equilibrium adsorption capacity toward the target molecule was investigated by placing 20 mg of TMMIPs/TMNIPs in 10 mL aqueous solution with various TC concentrations, ranging from 10 to 200 mg L^{-1}, and the temperature was kept at 45 °C in water bath. The adsorption amount of TMMIPs/TMNIPs could be obtained according to the deviation between the initial and the residual TC concentration in the solution, which was measured by a UV–Vis spectrophotometer at 276 nm. The equilibrium

adsorption amount of TC was calculated according to the following equation:

$$Q_e = \frac{(C_0 - C_e)V}{m} \quad (1)$$

where Q_e (mg g^{-1}) is the amount of TC adsorbed at equilibrium, C_0 and C_e (mg L^{-1}) are the concentration of TC at initial and equilibrium, respectively. V is the volume of TC solution, and m is the weight of absorbent.

Meanwhile, the adsorption kinetic studies were identical with those of equilibrium tests, the initial concentration was set as 100 mg L^{-1}, and the samples were separated at predetermined time intervals. The amount of TC adsorbed (Q_t, mg g^{-1}) was calculated according to the following equation:

$$Q_t = \frac{(C_0 - C_t)V}{m} \quad (2)$$

where C_t (mg L^{-1}) is the concentration of TC solution at any time t.

To study the selectivity property of the TC-imprinted composites, 20 mg of TMMIPs was placed into 10 mL each competitive antibiotic solution (TC, OTC, CAP and CIP) with the initial concentration of 100 mg L^{-1}. For comparison, the adsorption property of the TMNIPs was also investigated. All the experiments were carried out in triplicate.

Release experiments

TMMIPs/TMNIPs with loaded TC were separated magnetically, rinsed with water to reduce the non-specific adsorption and then eluted with 10 mL of methanol–acetic acid (9/1, v/v) at 20 °C for 360 min to release TC. The release amounts of TC were determined using an UV–Vis spectrophotometer.

Results and discussion

UV spectrum study of interaction between template and functional monomer

It is necessary to know how the functional monomers strongly interact with the template molecule by hydrogen bonding, ionic bonding or other interaction forces and form stable host–guest complexes prior to polymerization [34, 35]. When the template molecule and functional monomers formed complexes in solution for a certain time, the stability of these complexes reflected the affinity and selectivity of imprinted polymer to a degree. In this study, MAA was directly used as the functional monomers for the imprinting template molecule (TC). To demonstrate a comparison between different concentration monomers and

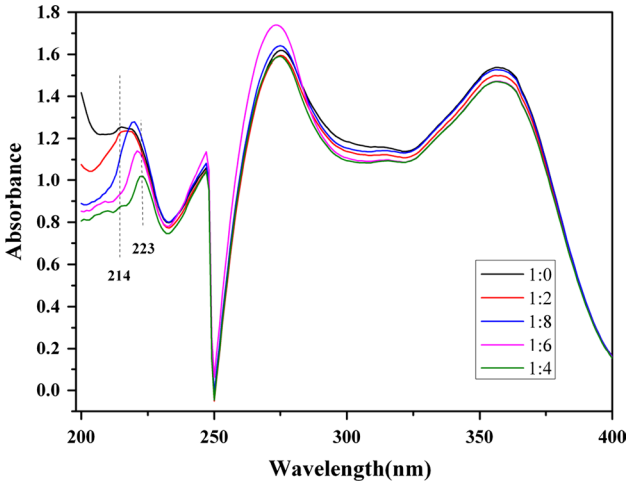

Fig. 2 UV spectrum study of interaction between template and functional monomer

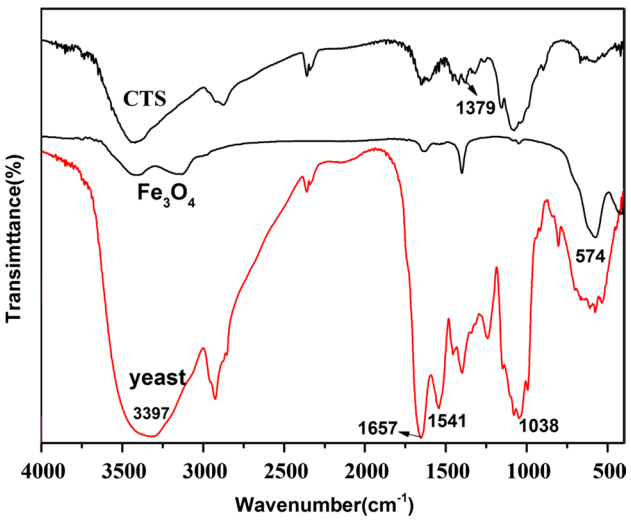

Fig. 3 FT-IR spectra of CTS, Fe_3O_4 and yeast

their suitability creation of recognition sites by molecular imprinting process, their ability to non-covalently interact with TC in a monomer mixture has been studied by UV difference spectroscopy and the results are shown in Fig. 2. It was clearly observed that the maximum absorption wavelength of TC at 214 nm in Fig. 2. Moreover, the maximum absorption wavelength showed changes in redshift due to functional monomer in the mixture solution. The result probably showed stable host–guest complex was synthesised between the template molecule (TC) and functional monomer (MAA) via chemical interaction in the solution. By analyzing Fig. 2, the optimal molar ratio of the template and functional monomer was 1:4, which was chosen for the synthesis of TMMIPs and TMNIPs.

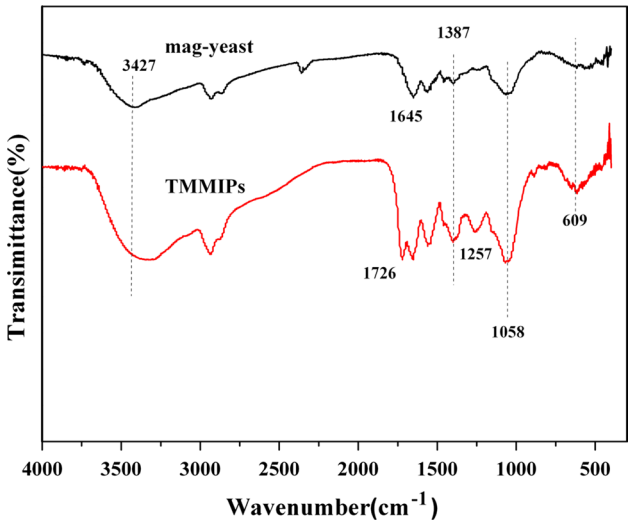

Fig. 4 FT-IR spectra of mag-yeast and TMMIPs

Characterization

Figure 3 displays the FT-IR spectra of Fe_3O_4, yeast and CTS, and as-prepared particles (such as mag-yeast and TMMIPs) are shown in Fig. 4. Compared with the FT-IR of yeast, the characteristic absorption peaks of the stretching vibrations of O–H and P–O for mag-yeast shifted to 3427 and 1058 cm^{-1}, respectively. Moreover, the strong peaks of amide I and amide II for yeast were displayed at 1657 and 1541 cm^{-1}, respectively. But the same peaks did not appear in the FT-IR spectra of mag-yeast, and the peak of amide bands I shifted to 1645 cm^{-1}, indicating that the presence of cross-linking reaction had occurred between the glutaraldehyde and the N atom of the yeast. In the FT-IR spectrum of mag-yeast, a sharp peak around 1377 cm^{-1} could be assigned to the CH_3 symmetrical angular deformation of the CTS [36]. The peaks at 609 cm^{-1} were assigned to Fe–O bond vibration of Fe_3O_4, which demonstrates the Fe_3O_4 was successfully introduced to mag-yeast and TMMIPs. The TMMIPs showed significant peaks around 1726 and 1257 cm^{-1}, which were assigned to C=O stretching vibration of carboxyl (MAA) and C–O symmetric stretching vibrations of ester (EGDMA), respectively. The results confirmed that the imprinted polymers were successfully coated on the surface of the mag-yeast [37].

Figure 5a presents TEM micrographs of Fe_3O_4 nanoparticles. The diameter of Fe_3O_4 nanoparticles is about 10 nm. Figure 5b presents SEM micrographs of mag-yeast. It can be seen that the surface of mag-yeast are rough; the mean size of the mag-yeast was obviously increased because of the coatings of CTS layers. SEM micrographs of the prepared TMMIPs are presented in Fig. 5c, d. It can be observed that the TMMIPs present a relatively rough surface, which could be attributed to the cavities left after the elution of the imprinting TC onto the cross-linked network.

Figure 6 shows the XRD patterns of the mag-yeast and TMMIPs. In the 2θ range of 20°–70°, six characteristic peaks of Fe_3O_4 ($2\theta = 30.2°$, 35.5°, 43.1°, 53.4°, 57.0° and 62.6°) were all observed in the mag-yeast and TMMIPs, and the peak positions could be indexed to (220), (311), (400), (422), (511) and (440) [JCPDS card (19-0629)]. The result revealed that the crystal structure of Fe_3O_4 remained steady in the polymerization reaction and the Fe_3O_4 was indeed integrated into TMMIPs [38].

Figure 7 gives the TGA curves of mag-yeast, TMMIPs and TMNIPs. For mag-yeast TMMIPs and TMNIPs, the weight loss of all the particles was low below 200 °C; the weight decrease was mainly attributed to the loss of physically absorbed water, which was 10.36, 2.95 and 7.53 % for mag-yeast, TMMIPs and TMNIPs, respectively. The rapid rate of weight loss in the temperature range between 200 and 800 °C was produced by the thermal decomposition of imprinted polymers. In this stage, there were no clear differences between the TMMIPs and TMNIPs, and the value of the mass loss was 65.03 and 65.58 %, respectively. The weight loss was very low above 800 °C, demonstrating the presence of only the thermal resistance of carbon particles and Fe_3O_4 within the temperature range.

Figures 8 and 9 show the magnetic hysteresis loop of mag-yeast and TMMIPs. Figures 8 and 9 show that the magnetization curves of two composites were symmetrical and passed through the origin with no hysteresis suggesting that the composites were super-paramagnetic. The saturation magnetization (Ms) values of mag-yeast and TMMIPs were 2.57 and 1.97 emu g^{-1} at room temperature, respectively. The Ms value of TMMIPs was lower than that of the mag-yeast because of the polymeric coating had avoided the magnetite. This magnetic property of the TMMIPs remained magnetic enough to meet the need of magnetic separation. In Fig. 9b, it can be seen that the TMMIPs were rapidly gathered to the wall of the vial under an external magnetic field, obtaining a clear and transparent solution.

UV–Vis adsorption has been proved to be a convenient and effective technique to characterize the thermosensitive transition of polymers [39]. The absorbance change of TMMIPs/TMNIPs aqueous solution at different temperatures was detected at 500 nm (Fig. 10). The results showed that TMMIPs/TMNIPs have the excellent temperature responsiveness. The lower critical solution temperature (LCST) values of TMMIPs and TMNIPs were 33.65 and 34.15 °C, respectively, which were higher than that of pure PNIPAM (around 32 °C [17]) because of the incorporation of hydrophobic cross-linker (EGDMA) or the restriction of movement of polymer chains imposed by rigid support [40]. The absorbance of TMMIPs increased with the temperature increasing, and the change trend of absorbance

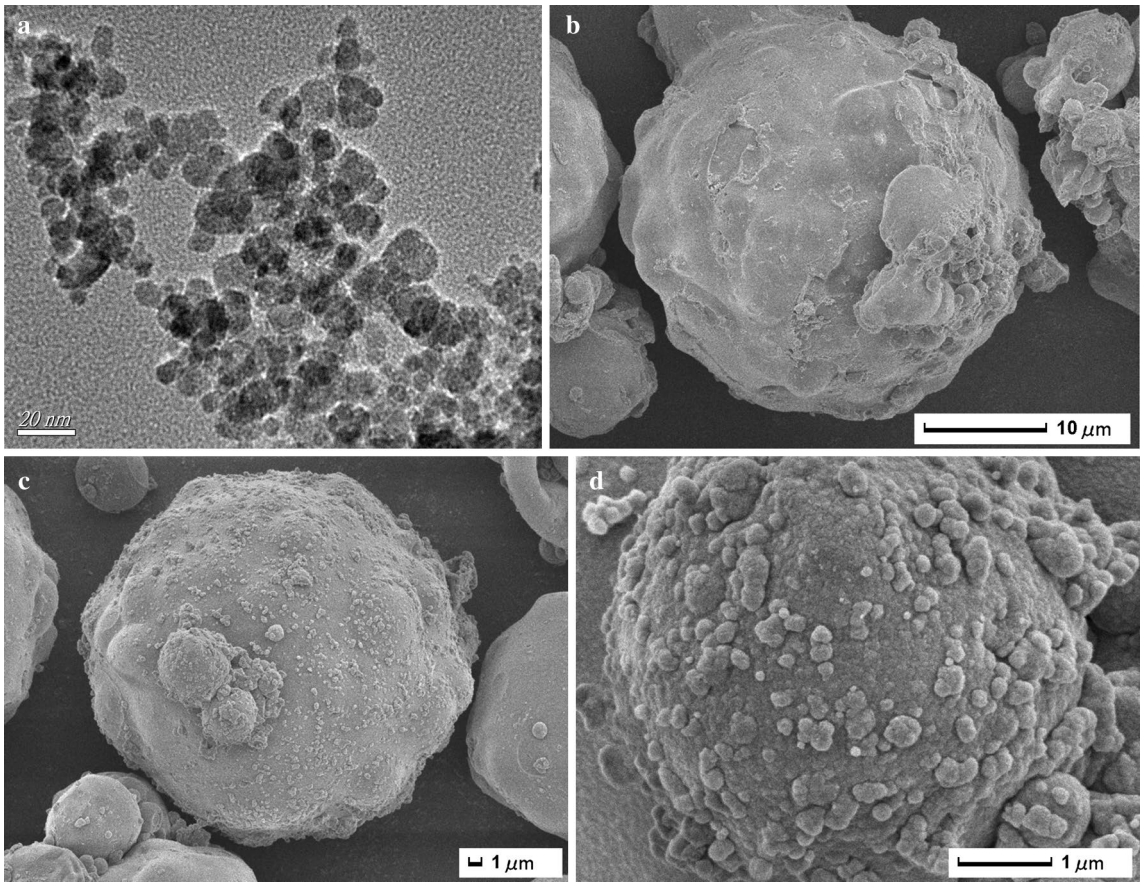

Fig. 5 TEM image of Fe_3O_4 nanoparticles (**a**) and SEM images of mag-yeast (**b**) and TMMIPs (**c**, **d**)

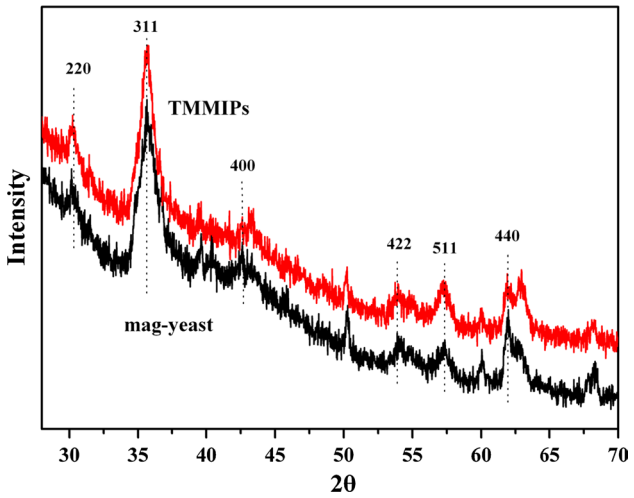

Fig. 6 Powder XRD patterns of mag-yeast and TMMIPs

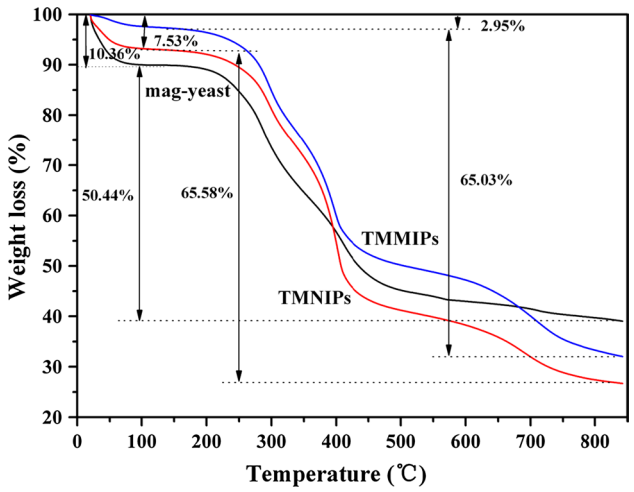

Fig. 7 TGA curve of mag-yeast, TMMIPs and TMNIPs

was similar to those of water solution of pure PNIPAM and dispersion of TMMIPs prepared by Yan's group [20], which was mainly attributed to the temperature-dependent solubility of PNIPAM in water.

Adsorption kinetic studies

Figure 11 shows the adsorption kinetics of the TMMIPs and TMNIPs adsorbents for TC. The adsorption capacity of the TMMIPs for TC was higher than the TMNIPs, showing

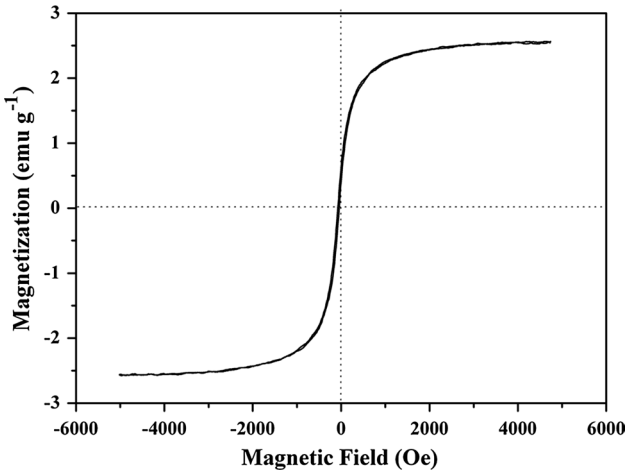

Fig. 8 Magnetization curves obtained by VSM at room temperature of mag-yeast

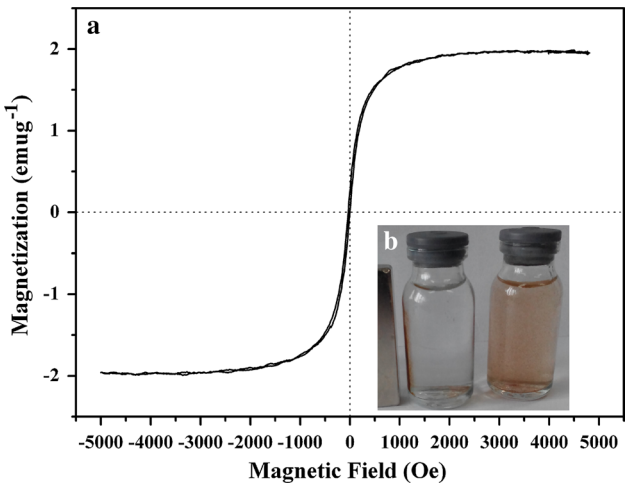

Fig. 9 Magnetization curves obtained by VSM at room temperature of TMMIPs (**a**) *inset*: a photograph of the TMMIPs dispersed in the water in the presence (*left*) and absence (*right*) of an external magnetic field (**b**)

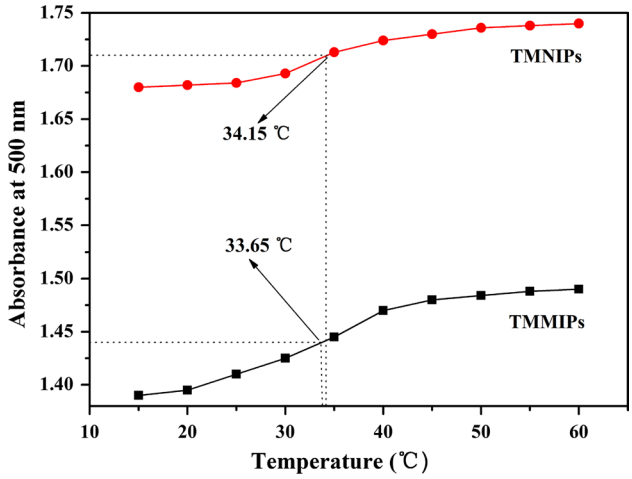

Fig. 10 Optical absorbance of TMMIPs and TMNIPs aqueous solution at various temperatures

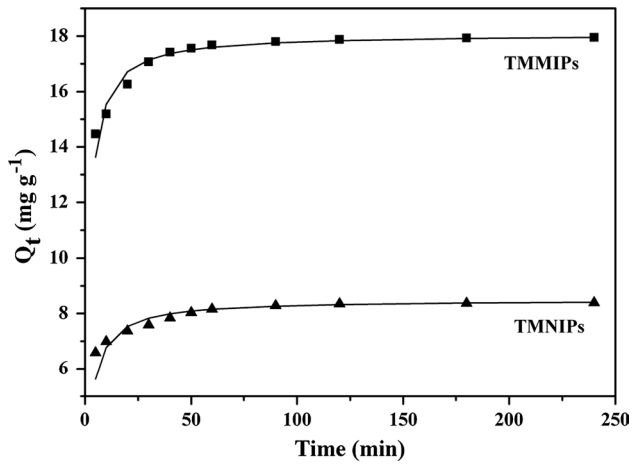

Fig. 11 Adsorption kinetic models of TMMIPs and TMNIPs

the good imprinting result of the TMMIPs for template molecule. In order to know the controlling mechanism of adsorption process of the TMMIPs and TMNIPs for TC, the pseudo-first rate equation and the pseudo-second rate equation were used to evaluate the experimental data obtained from batch adsorption experiments [41].

$$\ln (Q_e - Q_t) = \ln Q_e - k_1 t \quad (3)$$

$$\frac{t}{Q_t} = \frac{1}{K_2 Q_e^2} + \frac{t}{Q_e} \quad (4)$$

where Q_e (μmol g^{-1}) and Q_t (μmol g^{-1}) were the amounts of TC adsorbed on the adsorbent at equilibrium and time t, respectively, k_1 (min^{-1}) was the pseudo-first-order rate constant of adsorption, which was calculated from the plots of $\ln(Q_e - Q_t)$ versus t, and k_2 (g μmol^{-1} min^{-1}) was the rate constant of pseudo-second-order adsorption, which could be obtained from the plot of t/Q_t versus t.

In the light of the second-order model, the initial adsorption rate (h, μmol g^{-1} min^{-1}) and half-equilibrium time ($t_{1/2}$, min) are summarized in Table 1 and can be represented by [42]:

$$h = K_2 Q_e^2 \quad (5)$$

$$t_{1/2} = \frac{1}{K_2 Q_e} \quad (6)$$

The adsorption rate constants and linear regression values of the two rate equations are listed in Table 1. It can be

Table 1 Kinetic constants for the pseudo-first-order equation and pseudo-second-order equation at 318 K

Adsorbents	$Q_{e,exp}$ (mg g^{-1})	Pseudo-first-order model			Pseudo-second-order model				
		$Q_{e,c}$ (mg g^{-1})	k_1 (L min^{-1})	R^2	$Q_{e,c}$ (mg g^{-1})	k_2 (g mg^{-1} min^{-1})	R^2	h (g mg^{-1} min^{-1})	$t_{1/2}$ (min)
TMMIPs	18.10	1.663	0.0128	0.753	18.08	0.034	0.99	11.08	1.63
TMNIPs	8.45	1.151	0.0149	0.864	8.49	0.046	0.99	3.32	2.56

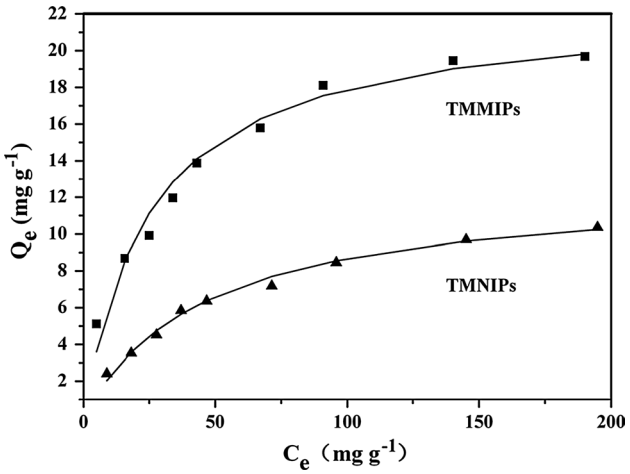

Fig. 12 Adsorption isotherms of TMMIPs and TMNIPs

seen that the pseudo-first-order model showed poor fitting with low regression coefficients value (R^2) and big variance between the experimental and theoretical values, while the pseudo-second-order model exhibited favorable fitting between experimental and calculated values of Q_e (R^2 values above 0.99), which was assumed that the adsorption of TC followed pseudo-second-order kinetics and chemical process could be the rate-limiting step in the adsorption process for TC and the adsorption capacity was proportional to the number of active sites on the adsorbent [43].

Adsorption isotherms study

The adsorption isotherm models are commonly used to evaluate the binding properties of TMMIPs and TMNIPs for TC. And the equilibrium data of the Langmuir and Freundlich isotherm models are shown in Fig. 12. The adsorption capacity of the TMMIPs for TC was higher than the TMNIPs, which suggested that the more efficient recognition sites located at the surface of TMMIPs. The Langmuir isotherm presupposes that the adsorption behavior was based on monolayer adsorption and the assumption of a structurally homogeneous adsorbent where all adsorption sites are identical. The Freundlich isotherm was an empirical equation which assumed a heterogeneous surface energy [44]. The nonlinear form of the Langmuir and Freundlich isotherm models was expressed by the following equations, respectively [45]:

$$Q_e = \frac{K_L Q_m C_e}{1 + K_L C_e} \tag{7}$$

$$Q_e = K_F C_e^{\frac{1}{n}} \tag{8}$$

where Q_e (mg g^{-1}) was the equilibrium adsorption capacity, C_e (mg L^{-1}) was equilibrium concentration of TC at equilibrium, Q_m (mg g^{-1}) was the maximum adsorption capacity of the adsorbent. K_L (L mg^{-1}) was the Langmuir adsorption constant, and K_F (mg g^{-1}) and n were both the Freundlich adsorption equilibrium constants.

The affinity between adsorbate and adsorbent can be predicted using the Langmuir parameter K_L from the dimensionless separation factor R_L,

$$R_L = \frac{1}{1 + C_m K_L} \tag{9}$$

where C_m is the initial TC concentration and K_L is the Langmuir isotherm constant. The adsorption process as a function of R_L may be described as follows: When R_L is greater than one, then the adsorption reaction is unfavorable, and it is linear when R_L is equal to one. When R_L is between zero and one, the reaction is favorable, while the reaction is supposed to be irreversible when R_L is equal to zero. All the calculated values of the adsorption experiment are listed in Table 2.

As can be seen from Fig. 12, the adsorption capacity increased with the increasing concentration of TC, and Q_m value of TMMIPs and TMNIPs was 22.47 and 12.66 mg g^{-1} at 318 K, respectively. It can be seen that the linear coefficients of determination (R^2) for the Freundlich isotherm model were lower than R^2 values for the Langmuir isotherm model in Table 2; the Q_m values for the adsorption of TC calculated from the Langmuir model were in close proximity to the experimental data. Obviously, the Langmuir model was much better to describe the adsorption of TC onto the TMMIPs than the Freundlich model.

Selectivity property of TMMIPs

To evaluate the binding selectivity of TMMIPs, three typical antibiotics including chemical structurally analogous

Table 2 Adsorption isotherm constants for TC adsorption onto TMMIPs and TMNIPs at 318 K

Adsorbents	Langmuir model				Freundlich model		
	$Q_{m,c}$ (mg g^{-1})	R_L	K_L (L mg^{-1})	R^2	K_F (mg g^{-1})	1/n	R^2
TMMIPs	22.47	0.113	0.0392	0.9943	2.9758	0.3847	0.9746
TMNIPs	12.66	0.187	0.0217	0.9944	0.9199	0.4788	0.9761

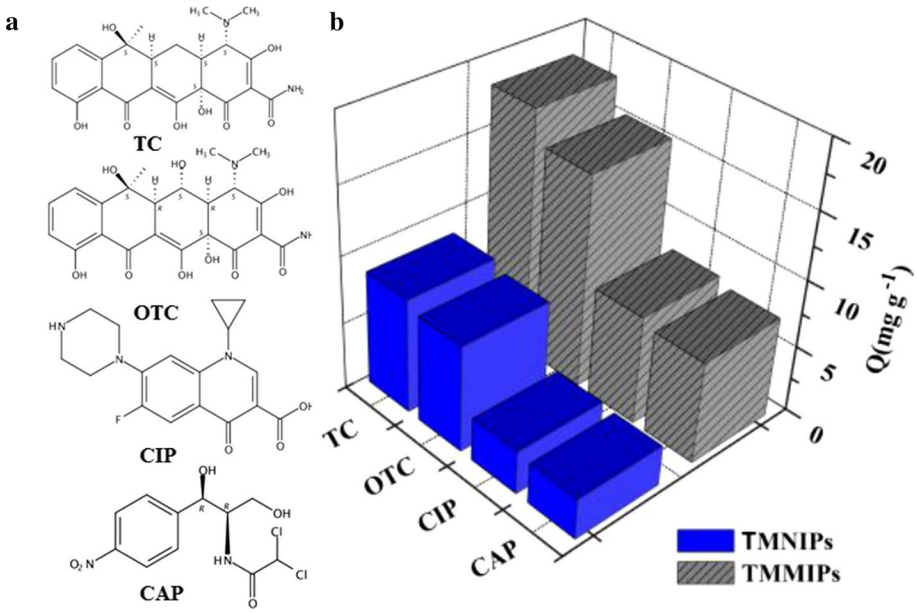

Fig. 13 Adsorption selectivity of the TMMIPs and TMNIPs

OTC and structurally different CAP and CIP were used as reference antibiotics. As shown in Fig. 13, the adsorption amount of TMMIPs for OTC was lower than for TC, which also showed a much larger adsorption capacity for TC than for the CAP and CIP molecules. Therefore, it can be concluded that the TMMIPs had good binding selectivity in the presence of interferent. Comparatively, the TMNIPs can be affected obviously by the interferent.

Optimization of release procedures

The temperature, solvents and time affected the reduction of the non-specific binding and the recovery of adsorbed compounds. At 20 °C, the PNIPAM polymer swelled, and the distance between curcumin and polymer network increased, and then the memory effect of curcumin would disappear, which will weaken the hydrophobic and hydrogen bonding interactions and then release curcumin completely [20]. However, the release time was relatively long (about 24 h [46]) while using the same solution with that in binding process. The washing step was an important step to remove the interferences with non-specific interaction and for selective extraction of target molecules [47]. The results are that polar and protic solvents decreased the non-covalent specific interactions between template molecules and TMMIPs and then reduced the affinity. Then, acetonitrile and methanol with different contents of acetic acid were selected to optimize washing and eluting solvents. The results indicated that components with non-specific interaction could be washed with acetonitrile, and then, about 97 % of TC was released by elution with methanol–acetic acid (9/1, v/v) with the optimum release time of 120 min (Fig. 14).

Reusability of TMMIPs

To investigate the regeneration ability of the TMMIPs, five adsorption/release cycles were performed. The adsorbed TC could be released when changing the temperature of aqueous solution rather than by using organic eluant [48], which presented solvent consuming and process tedious. The amounts of TC absorbed and released by TMMIPs in each cycle are depicted in Table 3. The experiments were all carried out at 20 °C. After five adsorption/release cycles, the results showed that the cycle time had a little influence on the binding and release ability of TMMIPs.

Conclusions

In conclusion, we developed an mild and effective method to prepare the thermal-responsive and magnetic

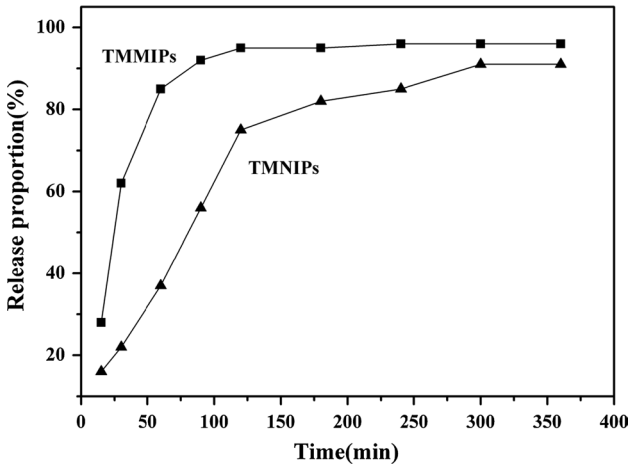

Fig. 14 TC release of TMMIPs with time in aqueous solution

Table 3 Adsorption capacity and release of TMMIPs in the regeneration process

Reusability cycles	Adsorption capacity (mg g^{-1})	Release (%)
0	18.1	98
1	17.8	96
2	17.6	94
3	17.3	93
4	17.1	92
5	17.0	90

Adsorbent dose: 0.01 g, solution volume: 10 mL, adsorption temperature: 318 K, release temperature: 293 K, initial concentration: 100 mg L^{-1}

molecularly imprinted polymers based on mag-yeast for selective adsorption and release of TC from aqueous solution. Imprinted polymerization reaction directly occured on the surface of mag-yeast. The equilibrium adsorption data of TMMIPs were well described by the Langmuir isotherm model. Pseudo-second-order kinetic model was used to fit the adsorption data well. The TMMIPs composed of PNIPAM that exhibited thermo-induced swelling/shrinking transition, and adsorption/release activities could accordingly be modulated by temperature. This work can be regarded as a perfect combination of selective adsorption, fast separation and controlled release. The obtained TMMIPs showed the good stability and regeneration property, which can be further applied in the drug release and separation of pollutants in aqueous environment.

Acknowledgments This work was financially supported by the National Natural Science Foundation of China (Nos. 21107037, 21176107), National Postdoctoral Science Foundation (No. 2013M530240), Postdoctoral Science Foundation funded Project of Jiangsu Province (No. 1202002B) and Programs of Senior Talent Foundation of Jiangsu University (No. 12JDG090), Key Scientific Programs of Higher Education of Henan Province of China (No. 15A150069), Youth Foundation of Pingdingshan University (No. 2012004), National Scientific Research Project Cultivating Foundation of Pingdingshan University (No. PYJJ2016005), Innovation Programs Foundation of Jiangsu Province (No. SJLX_0481).

References

1. J.D. Dai, Z.P. Zhou, X. Wei, J.M. Pan, T.B. Zou, C.X. Li, RSC Adv. **4**, 7967 (2014)
2. C. Nebot, M. Guarddon, F. Seco, A. Iglesias, J.M. Miranda, C.M. Franco, A. Cepeda, Food Control **46**, 495 (2014)
3. Q. Zhou, Y.Y. Zhang, N. Wang, L.H. Zhu, H.Q. Tang, Food Control **46**, 324 (2014)
4. L.L. Ji, Y.Q. Wan, S.R. Zheng, D.Q. Zhu, Environ. Sci. Technol. **45**, 5580 (2011)
5. N. Pastor-Navarro, Á. Maquieira, R. Puchades, Anal. Bioanal. Chem. **395**, 907 (2009)
6. J. Radjenovic, M. Petrovic, F. Ventura, D. Barcelo, Water Res. **42**, 3601 (2008)
7. V. Homem, L. Santos, J. Environ. Manag. **92**, 2304 (2011)
8. C. Reyes, J. Fernández, J. Freer, M.A. Mondaca, C. Zaror, S. Malato, H.D. Mansilla, J. Photochem. Photobiol. A **184**, 141 (2006)
9. L. Chen, W. Ma, J.D. Dai, J. Zhao, C.X. Li, Y.S. Yan, J. Photochem. Photobiol. A **328**, 24 (2016)
10. R. Daghrir, P. Drogui, Environ. Chem. Lett. **11**, 209 (2013)
11. A. Anglada, A. Urtiaga, I. Ortiz, J. Chem. Technol. Biotechnol. **84**, 1747 (2009)
12. J. Jeong, W. Song, W.J. Cooper, J. Jung, J. Greaves, Chemosphere **78**, 533 (2010)
13. M.M. Liu, L.A. Hou, S.L. Yu, B.T. Xi, Y. Zhao, X.F. Xia, Chem. Eng. J. **223**, 678 (2013)
14. P. Xu, G.M. Zeng, D.L. Huang, C.L. Feng, S. Hu, M.H. Zhao, Z.F. Liu, Sci. Total Environ. **424**, 1 (2012)
15. X.L. Gao, W. Xing, J. Zhou, G.Q. Wang, S.P. Zhuo, Z. Liu, Q.Z. Xue, Z.F. Yan, Electrochim. Acta **133**, 459 (2014)
16. M. Sánchez-Polo, I. Velo-Gala, J.J. López-Peñalver, Microporous Mesoporous Mater. **203**, 32 (2015)
17. W. Chen, Y. Ma, J. Pan, Z. Meng, G. Pan, B. Sellergren, Polymers **7**, 1689 (2015)
18. G. Pan, Q. Guo, C. Cao, H. Yang, B. Li, Soft Matter **9**, 3840 (2013)
19. Z.H. Meng, W. Chen, A. Mulchandani, Environ. Sci. Technol. **39**, 8958 (2005)
20. J.M. Pan, B. Wang, J.D. Dai, H. Hang, H.X. Ou, Y.S. Yan, J. Mater. Chem. **22**, 3360 (2012)
21. G. Pan, Q. Guo, Y. Ma, H. Yang, B. Li, Angew. Chem. Int. Ed. **52**, 6907 (2013)
22. C.B. Gong, M.H.W. Lam, H.X. Yu, Adv. Funct. Mater. **16**, 1759 (2006)
23. Y. Kanekiyo, R. Naganawa, H. Tao, Angew. Chem. Int. Ed. **42**, 3014 (2003)
24. J.X. Wang, J.M. Pan, Y.J. Yin, R.R. Wu, X.H. Dai, J.D. Dai, H.X. Ou, J. Ind. Eng. Chem. **25**, 321 (2015)
25. S.J. Li, S. Pilla, S.Q. Gong, J. Polym. Sci. Pol. Chem. **47**, 2352 (2009)
26. H. Tokuyama, S. Naohara, M. Fujioka, React. Funct. Polym. **68**, 182 (2008)
27. Q. Yao, Y. Zhou, J. Inorg. Organomet. Polym. Mater. **19**, 466 (2009)
28. Y.X. Zhou, B. Yu, E. Shiu, K. Levon, Anal. Chem. **76**, 2689 (2004)

29. X.Z. Xu, S.X. Chen, Q.H. Wu, J. Colloid Interface Sci. **385**, 193 (2012)
30. A. Terziyska, L. Waltschewa, P. Venkov, Environ. Pollut. **109**, 43 (2000)
31. H. Zhou, T.X. Fan, D. Zhang, Microporous Mesoporous Mater. **100**, 322 (2007)
32. W. Ma, J.D. Dai, X.H. Dai, Y.S. Yan, Mon. Chem. **146**, 465 (2015)
33. X.X. Li, J.M. Pan, J.D. Dai, X.H. Dai, X. Wei, Chem. Eng. J. **198**, 503 (2012)
34. M.J. Meng, Y.H. Feng, M. Zhang, Y.J. Ji, J.D. Dai, Y.S. Yan, Chem. Eng. J. **231**, 132 (2013)
35. M.J. Meng, Z. Wang, L. Ma, M. Zhang, J. Wang, X.H. Dai, Y.S. Yan, Ind. Eng. Chem. Res. **51**, 14915 (2012)
36. G.Y. Li, K.L. Huang, Y.R. Jiang, Int. J. Biol. Macromol. **42**, 405 (2008)
37. K. Yoshimatsu, K. Reimhult, A. Krozer, Anal. Chim. Acta **584**, 112 (2007)
38. Y.L. Zhang, J. Zhang, C.M. Dai, Carbohydr. Polym. **97**, 809 (2013)
39. C. Chang, H. Wei, J. Feng, Z.C. Wan, X.J. Wu, D.Q. Wu, R.X. Zhuo, Macromolecules **42**, 4838 (2009)
40. S.Y. Zhou, A.L. Xue, Y. Zhang, M.S. Li, J.G. Wang, Y.J. Zhao, W.H. Xing, J. Membr. Sci. **450**, 351 (2014)
41. X.M. Peng, D.P. Huang, T. Odoom-Wubah, D.F. Fu, J.L. Huang, Q.D. Qin, J. Colloid Interface Sci. **430**, 272 (2014)
42. L.C. Xu, J.D. Dai, J.M. Pan, X.X. Li, P.W. Huo, Y.S. Yan, Chem. Eng. J. **174**, 221 (2011)
43. G. Baydemir, M. Andaç, N. Bereli, Ind. Eng. Chem. Res. **46**, 2843 (2007)
44. X. Wang, J.M. Pan, W.S. Guan, J.D. Dai, X. Zou, Y.S. Yan, J. Chem. Eng. Data **56**, 2793 (2011)
45. J.M. Pan, X. Zou, X. Wang, W.S. Guan, Y.S. Yan, J. Han, Chem. Eng. J. **162**, 910 (2010)
46. L.C. Xu, J.M. Pan, J.D. Dai, X.X. Li, H. Hang, Z.J. Cao, Y.S. Yan, J. Hazard. Mater. **233**, 48 (2012)
47. D.L. Xiao, P. Dramou, N.Q. Xiong, H. He, H. Li, D.H. Yuan, H. Dai, J. Chromatogr. A **1274**, 44 (2013)
48. J.D. Dai, J.M. Pan, L.C. Xu, X.X. Li, Z.P. Zhou, R.X. Zhang, Y.S. Yan, J. Hazard. Mater. **205–206**, 179 (2012)